Computing the viscosity of supercooled liquids

Akihiro Kushima,[1] Xi Lin,[2,a)] Ju Li,[3,b)] Jacob Eapen,[4] John C. Mauro,[5] Xiaofeng Qian,[1] Phong Diep,[5] and Sidney Yip[1,c)]
[1]*Department of Nuclear Science and Engineering and Department of Materials Science and Engineering, Massachusetts Institute of Technology, Cambridge, Massachusetts 02139, USA*
[2]*Department of Mechanical Engineering and Division of Materials Science and Engineering, Boston University, Boston, Massachusetts 02215, USA*
[3]*Department of Materials Science and Engineering, University of Pennsylvania, Philadelphia, Pennsylvania 19104, USA*
[4]*Department of Nuclear Engineering, North Carolina State University, Raleigh, North Carolina 27695, USA*
[5]*Science and Technology Division, Corning Incorporated, Corning, New York 14831, USA*

(Received 15 September 2008; accepted 4 April 2009; published online 11 June 2009)

We describe an atomistic method for computing the viscosity of highly viscous liquids based on activated state kinetics. A basin-filling algorithm allowing the system to climb out of deep energy minima through a series of activation and relaxation is proposed and first benchmarked on the problem of adatom diffusion on a metal surface. It is then used to generate transition state pathway trajectories in the potential energy landscape of a binary Lennard-Jones system. Analysis of a sampled trajectory shows the system moves from one deep minimum to another by a process that involves high activation energy and the crossing of many local minima and saddle points. To use the trajectory data to compute the viscosity we derive a Markov Network model within the Green–Kubo formalism and show that it is capable of producing the temperature dependence in the low-viscosity regime described by molecular dynamics simulation, and in the high-viscosity regime (10^2–10^{12} Pa s) shown by experiments on *fragile* glass-forming liquids. We also derive a mean-field-like description involving a coarse-grained temperature-dependent activation barrier, and show it can account qualitatively for the fragile behavior. From the standpoint of molecular studies of transport phenomena this work provides access to long relaxation time processes beyond the reach of current molecular dynamics capabilities. In a companion paper we report a similar study of silica, a representative *strong* liquid. A comparison of the two systems gives insight into the fundamental difference between strong and fragile temperature variations. © *2009 American Institute of Physics*. [DOI: 10.1063/1.3139006]

I. INTRODUCTION

The viscosity of a liquid is a measure of shear stress relaxation, being a product of the shear modulus and a structural relaxations time. When viscosity increases strongly with lowering temperature, the behavior is attributed to a rapidly increasing relaxation time, the onset of slow dynamics. Two challenges arise in connection with this ubiquitous phenomenon. One is conceptual—slow dynamics has implications for the fundamental understanding of the glass transition. The other is computational—how can one calculate the viscosity directly from knowledge of molecular structure and intermolecular interaction. This work addresses the latter challenge by proposing a method to compute the viscosity over a range of values where atomistic methods have not been able to reach to date. As may be expected, our results also have implications for the slow dynamics of supercooled liquids.

Many liquids, upon undercooling, exhibit a super-Arrhenius shear viscosity behavior over a narrow temperature range, a characteristic known as fragility.[1] The fragile behavior of viscosity is a problem of considerable interest to molecular-level calculations that attempt to sample the underlying potential energy surface (PES).[2,3] While the minima of the PES (inherent structure)[4] and saddle points can be found by various numerical procedures,[3] no method yet exists that can compute the viscosity behavior over the range from 10^2 to 10^{12} Pa s.

In this work we describe a sampling algorithm for complex PES which allows the system to climb out of an arbitrary series of potential wells following a minimum energy path. Laio and Parrinello showed how one can apply energy penalty functions to activate the system to constantly explore new regions of phase space, and used this procedure in conjunction with molecular dynamics (MD) to study molecular reactions[5] and structural phase transitions.[6] We have coupled this algorithm of activation through energy penalty function with static relaxation to study the transition state pathways (TSPs) of supercooled liquids, after first testing its effectiveness in reproducing the activation barriers for adatom and adcluster diffusion on metal surfaces.[7] For a systematic application of the TSP trajectory we reformulate the Green–Kubo expression for the shear viscosity to use a Markov Network model to describe the kinetics of hopping between

a)Electronic mail: linx@bu.edu.
b)Electronic mail: liju@seas.upenn.edu.
c)Electronic mail: syip@mit.edu.

local energy minima. We also discuss an approach to extract an effective activation barrier from an analysis of the TSP trajectory sampled which can be used, in the heuristic spirit of transition state theory, to describe the temperature variation of the shear viscosity of highly viscous liquids. For both formulations we obtain results for the binary Lennard-Jones (BLJ) model[8] that can qualitatively account for the observed features of fragile liquids. In a companion paper we report a similar study of silica, known for its representative strong liquid behavior in viscosity. Taken together, the results reveal how the difference between strong and fragile glass formers can be traced to the roughness of the PES, thus providing quantitative computational support for the usefulness of the landscape perspective.[9,10]

II. INHERENT STRUCTURE AND QUENCH PROBABILITY

We denote the potential energy of an N-particle system as $\Phi(\underline{r})$, where $\underline{r} \equiv (\underline{r}_1, \underline{r}_2, \ldots, \underline{r}_N)$ is a $3N$-dimensional vector specifying the system configuration. The $3N$-dimensional PES consists of a number of local minima (potential wells) superimposed on deeper and wider energy undulations (basins). The minima and basins are surrounded by saddle points (barriers) as special energies for the system to be activated out of or into the various potential wells.[9,11] The Φ hypersurface has a multitude of local minima, which can be described as a discrete set α, $\{\alpha\} \equiv (\alpha_1, \alpha_2, \ldots)$. The mapping of the $3N$-dimensional continuum to the discrete of minima $\{\alpha\}$ was introduced by Stillinger and Weber,[12] it is implemented by direct energy minimization ("quenching") from any point in configuration space along a steepest descent path to the nearest local minimum.

Although the inherent structure approach represents a way to partition the PES into a set of local energy minima $\{\alpha\}$, the information contained in $\{\alpha\}$ alone is not sufficient to perform calculation of all physical properties. For example, it does not give any information about the barriers between the minima.[13] On the other hand the method described in this work does take advantage of the information available. We consider the specific model of a BLJ system.[8] We use a periodic simulation cell of 100 particles with $A:B$ ratio of 80:20, and reduced density of 1.2 interacting with $V_{\alpha\beta}(r) = 4\varepsilon_{\alpha\beta}[(\sigma_{\alpha\beta}/r)^{12} - (\sigma_{\alpha\beta}/r)^6]$, where $\alpha, \beta \in \{A, B\}$. The parameters of the potential are given as $\varepsilon_{AA}=1.0$, $\varepsilon_{AB}=1.5$, $\varepsilon_{BB}=0.5$, $\sigma_{AA}=1.0$, $\sigma_{AB}=0.8$, and $\sigma_{BB}=0.88$. All radius cutoffs are taken to be $2.5\sigma_{AA}$. Using this cutoff radius and the density, we have not observed significant box size effects on the computed mean square displacement curves for systems with 100 and 500 particles.

Figure 1 shows the energy spectra $\{E(\alpha)\}$ generated by taking constant-volume MD simulations at several temperatures T and performing energy minimization at various points along each trajectory. Each quench produces a local minimum energy and a corresponding system configuration. We see the values of the local minima span a wide energy range at high T ($T=5.0$) which decreases somewhat at an intermediate temperature $T=0.5$. Below this value the local minima are strongly clustered in a very narrow energy range,

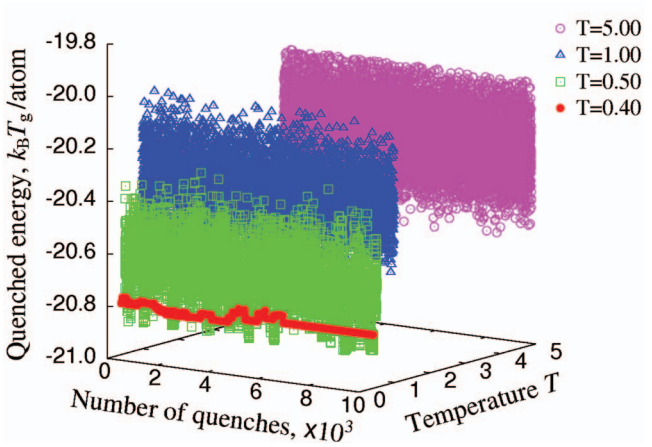

FIG. 1. (Color) Range of local minimum energies (inherent structure) sampled by steepest descent quench of constant-T MD trajectories at several temperatures. 10 000 quenches are performed at intervals of 10 000 MD steps. T_g is 0.37 in reduced unit.

implying the onset of limited atomic displacements in the system.[10] The clustering of inherent structure energy therefore is characteristic of slow dynamics which already can be inferred from a study of $\{\alpha\}$ by MD.

The existence of a characteristic temperature below which the clustering of $\{E(\alpha)\}$ is a qualitative aspect of supercooled liquids relevant to the present work. To develop this concept further one can define the quench probability $f(E|T)$ as a statistical distribution of inherent structure energy at a given T.[14] Figure 2(a) shows several such distributions for the present BLJ model, while Fig. 2(b) shows the temperature variation of average inherent structure energy, a behavior we have already noted in Fig. 1. Through $\bar{E}(T)$ one can discuss the effects of cooling rate.[10,11] Figure 2(b) is significant in our argument to obtain a temperature-dependent activation barrier because one can regard $\bar{E}(T)$ as an effective well depth of the PES; as we will see in Sec. IV its variation with T provides a mapping between the depth of an energy minimum and the temperature at which the PES trajectory is being sampled.

III. BASIN FILLING ALGORITHM

We have implemented a method to lift the system out of any potential well by a series of activation-relaxation steps. Our algorithm is a modification of that introduced by Laio and Parrinello[5] for escaping from free-energy minima, a method which has been called metadynamics.[6] Consider starting the process with the system in a selected local minimum $E_{\min}$ with corresponding atomic configuration at $\underline{r}_{\min}$. From this initial state the activation step drives the system away from its current configuration by imposing a prescribed energy penalty function (specified below), followed by a relaxation step to allow the system to settle into a new energy-minimized configuration in the presence of the penalty function. This process enables the system to start climbing out of its initial local minimum state $E_{\min}$. At the end of each activation-relaxation sequence, the system will find itself in a new relaxed atom configuration with a new energy. This process of activation relaxation is repeated until the system finds

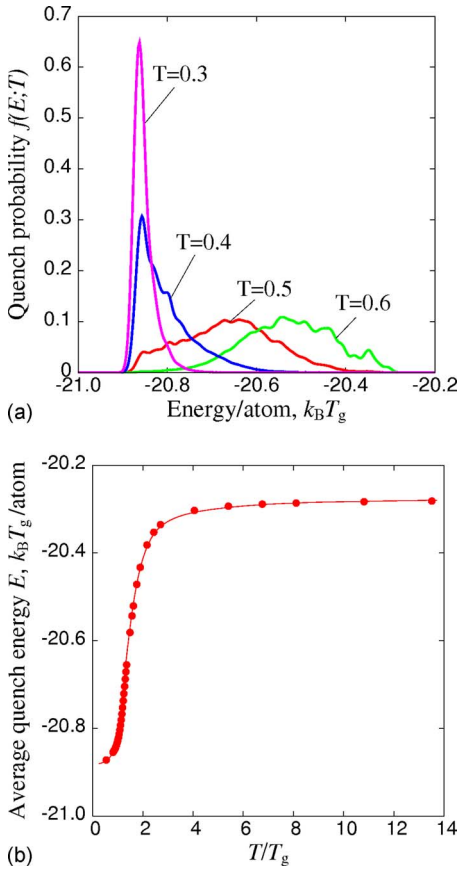

FIG. 2. (Color online) (a) Quench probability at different temperature. Curve for $T=0.5$ is constructed from the data shown in Fig. 1, which is then used to determine the other curves by quench probability scaling (Ref. 14). (b) Variation of average local minimum energy $\bar{E}(T)$ with temperature calculated from results such as those shown in (a). Note $\bar{E}(T)$ is constant at high temperature, but decreases sharply below $T \sim 2T_g$. T_g is 0.37 in reduced unit.

itself in a new local minimum which satisfies the condition (e) described below. With this new local minimum and the corresponding system configuration one can backtrack along the minimization path to deduce the saddle point E_{sad} and its configuration. The sequence of starting from an initial local minimum $E_{\mathrm{min}}^{(i)}$ to cross a saddle point $E_{\mathrm{sad}}^{(i)}$ to reach a nearby local minimum $E_{\mathrm{min}}^{(i+1)}$ can be repeated to generate a trajectory $\Gamma(E_{\mathrm{min}},E_{\mathrm{sad}}) \equiv (E_{\mathrm{min}}^{(1)},E_{\mathrm{sad}}^{(1)},E_{\mathrm{min}}^{(2)},E_{\mathrm{sad}}^{(2)},\cdots)$. Figure 3 depicts such a process for three local minima and two saddle points.

The algorithm for the basin-filling method thus can be specified as follows.

(a) Select an initial local minimum $E_{\mathrm{min}}^{(1)}$ (can choose an inherent structure energy from $\{\alpha\}$) and corresponding system configuration, say $\underline{r}_{\mathrm{min}}^{(1)}$.
(b) Activation step—apply a penalty function $\phi_1(r) = W \exp[-(\underline{r}-\underline{r}_{\mathrm{min}}^{(1)})^2/2\sigma^2]$, such that total system energy becomes $\Phi_{\mathrm{p}}^1 = \Phi + \phi_1$. W and σ are prescribed constants which determine the strength and the penalty and spatial extent of the activation, respectively.
(c) Relaxation step—minimize Φ_{p}^1 to obtain new energy and configuration $\underline{r}_{\mathrm{min}}^{(2)}$.
(d) Repeat (b) and (c) with $\Phi_{\mathrm{p}}^2 = \Phi_{\mathrm{p}}^1 + \phi_2$, $\Phi_{\mathrm{p}}^3 = \Phi_{\mathrm{p}}^2 + \phi_3, \ldots$ until a new local minimum is identified as specified in (e).

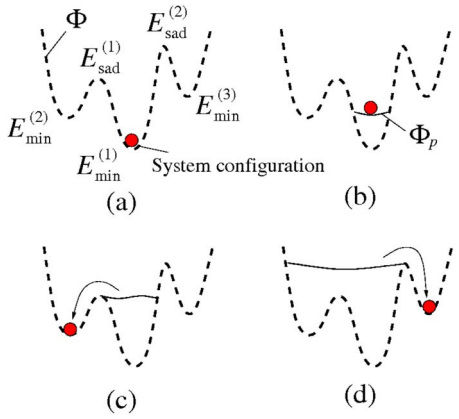

FIG. 3. (Color online) Schematic illustration explaining the basin-filling method. Dashed and solid lines indicate original PES and penalty potential, respectively. Penalty functions push the system out of a local minimum to a neighboring minimum by crossing the lowest saddle barrier.

(e) Confirm the sampling of a new local minimum $E_{\mathrm{min}}^{(2)}$ and configuration $\underline{r}_{\mathrm{min}}^{(2)}$ by checking to ensure that both $\partial\Phi/\partial\mathbf{r}(\underline{r}_2^m)=0$ and $\phi_{\mathrm{p}}(\underline{r}_2^m)=0$ are satisfied.
(f) Backtrack the minimization path to identify the saddle point and its energy E_{sad}.
(g) Repeat processes from (b) to (f) until sufficiently large configurational space has been sampled.

Notice that when the penalty functions are added to the system, as long as the system has not climbed out of the well, there will be a difference between Φ_p and Φ. When the system does escape from the well and goes into a new minimum, one cannot tell from looking at Φ_p and Φ alone, but their difference should be essentially zero. One needs to check after every relaxation to see if the two conditions listed in (e) are satisfied. If they are both satisfied, this means the system is indeed in a new minimum. If not, that means the system has not escaped. The two conditions are necessary and sufficient, while the vanishing of the difference between Φ_p and Φ is necessary but not sufficient. We do not specify the search direction as in the dimer method.[7] By keeping all the Gaussian penalty functions imposed during the simulation, we eliminate frequent recrossing of small barriers, which is a significant advantage of the history-penalized basin-filling methods.[5,15] However this type of methods could suffer from poor scaling with system size or number of particles participating in the activation and relaxation. In principle, it may seem that the number of penalty functions needed to perform adequate sampling could grow exponentially with the configuration space dimension. We have found this is not the case in the filling of glassy basins because the volume of configuration space to be sampled is much smaller than that of the entire system. The reduction arises from the particles being effectively constrained to their local atomic positions. For a crystal where each atom occupies $(x\%)^3$ of the configuration space, the volume to be sampled is $(x\%)^{3N}$. From the Lindemann criterion for melting,[16] an estimate of $x\%$ is approximately 0.13 for face-center-cubic crystals. For the BLJ liquid the range of atomic mobility may be obtained from the mean square displacement determined by MD simulation.[8] The mean square displacement shows quadratic

dependence on time at short times which corresponds to short-time ballistic motion of particles. At intermediate times, the mean square displacement levels off to a plateau over several decades because the particle is trapped in the cage formed by the neighboring particles that surround it. Once the system gets out from this cage the mean square displacement starts to increase again. From Ref. 16, one can estimate the size of the cage to be $\langle r^2(t)\rangle \sim 0.1$. We therefore chose $\sigma^2=0.1$ corresponding to the estimated cage size. Using penalty functions with σ estimated in this manner we found that about 2000 penalty functions are sufficient to fill the lowest minimum found in the inherent structure analysis using simulation cells containing 100 and 256 particles. The local minimum well is known to have a volume that depends on the energy, the volume becoming exponentially large as the energy is lowered.[17] Therefore, σ needs to be modified according to the energy region of PES sampled (smaller σ for high Φ and larger σ for low Φ) in order to escape a single local minimum. On the other hand we are not interested in activation process for escaping from each local minimum but in escaping from a broad collection of several minima (the basin or cage). Our experience shows that a compromise is to choose a fixed value of σ to be the estimated size of the cage.

We should emphasize that in our method the system moves in the energy space Φ_p which is the sum of the original potential and the penalties that have been applied up to that point. Since the corresponding system configurations at any stage of the activation and relaxation step is known, we can always display the trajectory track in Φ-space. The distinction between Φ and Φ_p is essential to understanding the results of our algorithm. With the energy landscape sampling proceeding under the dynamics governed by Φ_p, we may consider our method to be based on so-called metadynamics.[5] Moreover, the sampled trajectory consisting of local minima and saddle points will be displayed only in Φ-space so it is meaningful to compare our results with those obtained using other methods such as hyperdynamics or adaptive kinetic Monte Carlo. This point is further discussed in Appendixes A and B where we discuss benchmarking the results of the basin-filling method.

A typical trajectory generated by the algorithm just described, applied to a system of 100 particles interacting through the BLJ potential[8] with periodic boundary condition, is shown in Fig. 4, using a value of $W=1.0$ and $\sigma^2=0.1$ in reduced units. The sampling started in a low-energy minimum denoted by (a). The energy and corresponding atomic configurations at this state were obtained from an inherent structure calculation at $T=0.5$ (see Fig. 1). One sees a number of general features of this PES trajectory, particularly the irregular and appreciable fluctuations between local minima and saddle points. This particular trajectory shows two deep minima (basins), marked as (a) and (b), which are well separated along the trajectory. The overall appearance of the trajectory is one of roughness.

One can ask about the extent to which the sampled trajectory depends on the initial local minimum. Suppose one does not start at such a deep minimum, what changes can be expected in the sampling? Figure 5 shows two other trajectories which started at local minima with higher energies

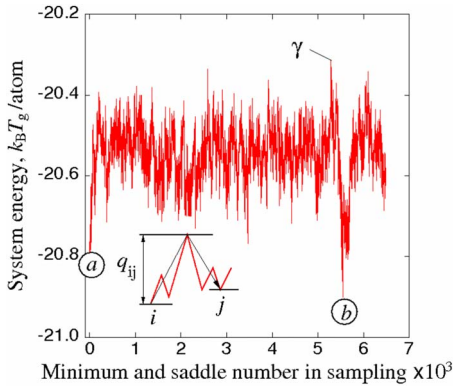

FIG. 4. (Color online) Trajectory generated from basin filling sampling. Activation barrier between minimum i and j q_{ij} is defined by smallest saddle point between them. T_g is 0.37 in reduced unit.

than state (a) in Fig. 4. Qualitatively speaking, the trajectories connecting basins in higher energy region with more shallow well depths tend to have smaller fluctuations.

Our interest lies primarily in quantifying the connectivity of the local minima through the saddle points. This information is embedded in any trajectory describing the hopping from one major basin to another. Figure 6 is a way of displaying the topological connectivity in a tree structure, the so-called disconnectivity graph.[13] In this figure each local minimum is represented by an end point of the vertical line and a saddle point by a vertex point, the results being taken from Fig. 4. The lower tip of a vertical line indicates value of that local minimum, and vertical lines end at vertex points to connect to other minima. We see that the connection between deep minima a and b requires high activation energy at point γ and involves many steps (intermediate saddles). On the other hand, local minima which are less deep can connect at lower vertex points.

The overall appearance of Fig. 6 is consistent with our observation that the trajectory in Fig. 4 has a relatively com-

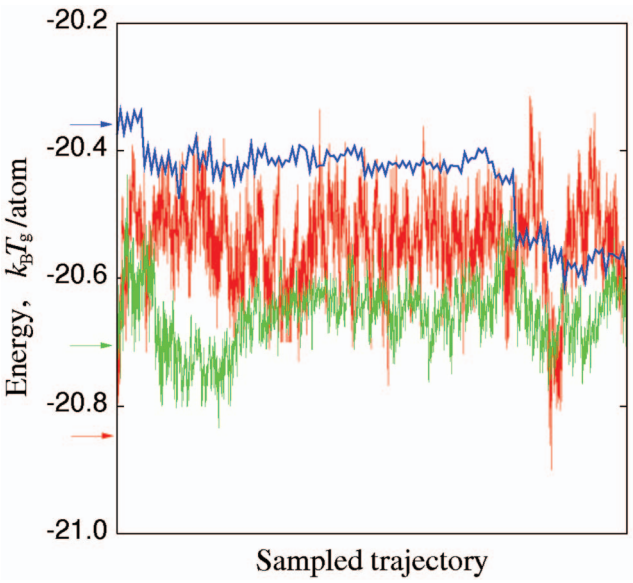

FIG. 5. (Color) Basin filling sampling trajectories calculated from high (blue), intermediate (green), and low (red) energy minimum as initial configuration. T_g is 0.37 in reduced unit.

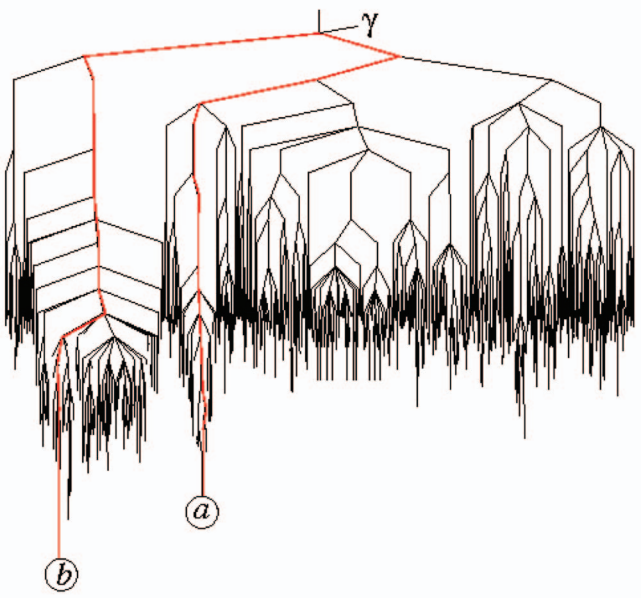

FIG. 6. (Color) Tree diagram connecting sampled minima and saddle points generated from the trajectory data of Fig. 4. Deep minima a and b are connected only through a high energy saddle γ. T_g is 0.37 in reduced unit.

plex connectivity topology. We will return to discuss this point further in connection with a companion paper on the connectivity structure of fragile versus strong liquids.

IV. COMPUTING VISCOSITY VIA TRANSITION STATE PATHWAY SAMPLING: NETWORK MODEL

In statistical mechanics thermal transport coefficients of fluids are generally expressed as integrals of time correlation functions in linear response theory (Green–Kubo formalism).[18,19] The shear viscosity η is given by a time integral

$$\eta(T) = \frac{V}{k_B T}\int_0^\infty \left\langle \sum \sigma^{xy}(t)\sigma^{xy}(0)\right\rangle dt, \tag{1}$$

where V denote the volume of the simulation cell maintained at temperature T, and the shear stress tensor is

$$\sigma^{xy} = \frac{1}{V}\left[\sum_j m_j v_j^x v_j^y + \frac{1}{2}\sum_{i\neq j} r_{ij}^x F_{ij}^y\right], \tag{2}$$

where F is the force between two atoms i and j, r is the position vector, and v is the velocity. x and y are two normal directions. There should be $\langle\sigma^{xy}\rangle=0$ for an ergodic liquid. In a finite-length numerical calculation, however, we enforce the above constraint by subtracting off the mean stress: $\sigma^{xy} \rightarrow \sigma^{xy}-\langle\sigma^{xy}\rangle$, so σ^{xy} in (1) stands for stress fluctuation around the mean. For simplicity we will suppress the superscript xy and introduce the time-dependent stress autocorrelation function $S(t)=\langle\sigma(t)\sigma(0)\rangle$. Because in dense gases and normal liquids $S(t)$ decays on the microscopic time scale of molecular collisions, it can be readily evaluated by MD simulation.[19] This situation will be considered further in Sec. V. In the supercooled regime the relevant dynamics is system activation over deep energy minima. Then $S(t)$ no longer decays on the time scale of intermolecular collisions and MD becomes ineffective. To overcome this difficulty we resort to activated state kinetics, provided by the TSP trajectories discussed in Sec. III. In this section we describe two formulations which make use of the TSP trajectory data to calculate viscosity in the $(1-10^{12}$ Pa s) range. Although differing in appearance, they are related in that one represents a simplification of the other.

A. Network model

We follow the Green–Kubo formalism but analyze $S(t)$ by treating basin hopping as a random walk on a Markov network of nodes.[20] We imagine the system is able to sample a number of deep minima within the timescale of the calculation so the average macroscopic properties such as viscosity can take on steady state values. We also assume the activation barriers for hopping are sufficiently high compared to k_BT, and the energy dissipation sufficiently efficient that after each hop the system loses memory of its previous history. Under these conditions we may take the hopping rate from nodes i to j to be given by transition state theory,

$$a_{ij} = \nu_o \exp(-Q_{ij}/k_BT), \tag{3}$$

where ν_o is a characteristic attempt frequency and Q_{ij} is the activation energy for transition from node i to node j. One can show[20] that in this model the stress correlation function becomes

$$\langle\sigma(t+\tau)\sigma(t)\rangle = \sum_i P_i\sigma_i g_i(\tau), \tag{4}$$

where P_i is probability the system is on node i, σ_i is the shear stress if the system is on node i (so-called *inherent stress*), and $g_i(\tau)$ is the average value of the shear stress at time τ given that the system has hopped to node i at time $t=0$. Taking advantage of the assumed Markov nature of the hopping process, an integral equation can be set up for $g_i(\tau)$ and solved without approximation,

$$g_i(\tau) = \int_0^\tau d\tau' s_i(\tau')\sum_j a_{ij}g_j(\tau-\tau') + s_i(\tau)\sigma_i, \tag{5}$$

where $s_i(t)=\exp(-a_i t)$ is the probability that the system will stay at node i during time t, and $a_i=\Sigma_j a_{ij}$ is rate at which the system will leave node i. To calculate the viscosity we need only the time integral of the correlation function, as indicated in Eq. (1). The result is (further details are given in Ref. 20)

$$\eta(T) = \frac{V}{k_BT}\sum_i P_i\sigma_i\frac{(\mathbf{A}(\omega=0^+)^{-1}\boldsymbol{\sigma})_i}{a_i}, \tag{6}$$

where $\mathbf{A}(\omega)$ is the matrix $(A)_{ij}\equiv\delta_{ij}-a_{ij}/(\omega+a_j)$, and $\boldsymbol{\sigma}$ is a vector with $(\boldsymbol{\sigma})_i\equiv\sigma_i$. Equation (6) gives the viscosity in terms of the nodal activation energy Q_{ij}, the energy of the nodes, E_i, for determining $P_i=\exp(-E_i/k_BT)/\Sigma_j\exp(-E_j/k_BT)$, and the stress if trapped in basin i,[20]

$$\sigma_i = \langle\sigma^{xy}\rangle_{\text{basin } i}, \tag{7}$$

with σ^{xy} from Eq. (2). Consider the special case of a two-state model, where $P_1=P_2=1/2$, $\sigma_1=-\sigma_2=\sigma_o$, and $a_{12}=a_{21}=\nu_0\exp(-Q/k_BT)$. Then Eq. (6) reduces to

$$\eta = \sigma_0^2 \nu_o^{-1} \exp(Q/k_B T). \quad (8)$$

B. Single path approximation

Equation (8) has the form of an expression that has been widely used to correlate experimental data on viscosity,[21]

$$\eta(T) = \eta_0 \exp[\bar{Q}(T)/k_B T]. \quad (9)$$

Equation (9) was first used by Andrade as a two-parameter formula to describe liquids, the prefactor η_o and the activation barrier $\bar{Q}$ were treated as fitting constants.[21] In contrast we adopt Eq. (9) as a temperature-dependent relation between the viscosity and an effective activation barrier to be extracted from appropriate TSP trajectory data. The analysis which we will carry out to obtain $\bar{Q}(T)$ is discussed in detail in Appendix B.

In our work Eq. (9) thus becomes a method to calculate $\eta(T)$. Because of the way we extract $\bar{Q}(T)$, it will be called the single path approximation (SPA) (see Appendix B). Henceforth we regard Eqs. (6) and (9) as two complementary formulations. They are predictive in that no experimental input is used in their evaluations. On the other hand, in order to compare the numerical results with MD simulations or experimental data, as we will discuss in Secs. V and VI, a normalization is required because transition state theory has been assumed in the formulations. The normalization amounts to choosing a value for ν_o in Eq. (3), or η_o in Eq. (9).

From our derivation of the Network model, Eq. (9) emerges as an approximation where viscous relaxation can be described by a single effective barrier. It can be seen in Appendix B that $\bar{Q}(T)$ has a thermodynamic component arising from the temperature variation of the average inherent structure energy, as discussed in Sec. II, as well as a kinetics component associated with the activation barrier analysis discussed in Appendix B.

The connection between the Network model and SPA is clearly brought out by Eq. (8) which shows the former reduces to the latter when there is only one activation path. In other words, SPA is a simplification of the Network model by ignoring all the correlations (coupling effects) among the different activation paths. One can think of another way to correct the SPA formulation, namely, entropy effects.[22,23] This may be implemented by modifying the activation barrier $\bar{Q}(T)$ in Eq. (9) to introduce a degeneracy factor $G(T)$ in the form of an Adam–Gibbs relationship,[24]

$$\eta(T) = \eta_0 \exp[\bar{Q}(T)/\{k_B T \log G(T)\}], \quad (10)$$

with $G(T)$ being estimated from the density of states $G(E_i)$ distribution of the BLJ model given by Heuer.[24] The effect of this correction will be discussed along with the detailed implementation of Eq. (6).[20]

We will test our viscosity formulations in two ways. The first is to compare results with Green-Kubo MD, which is feasible only at low-viscosity values (Sec. V). Nonetheless, this is worthwhile because it constitutes a consistent benchmark where the same interatomic interaction model is used.

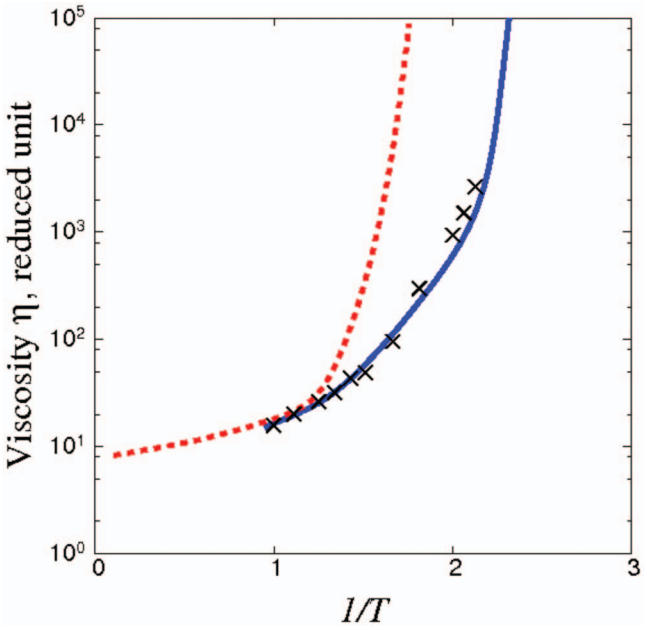

FIG. 7. (Color) Comparison of the shear viscosity calculated using the Network model (solid curve) and SPA formulation (dashed curve) with results obtained by MD simulation (crosses). All results are expressed in reduced units appropriate to the BLJ interatomic potential. Larger systems (2048 atoms) were used for the MD simulations.

The second test is to compare results with experimental data in the intermediate to high-viscosity range ($1-10^{12}$ Pa s) (Sec. VI). In this comparison we need to keep in mind that our results are obtained using the BLJ model potential which does not necessarily describe any real liquid.

V. VISCOSITY AT HIGH TEMPERATURES: COMPARISON WITH MOLECULAR DYNAMICS

At temperatures near the normal liquid range the viscosity values are low enough for conventional MD to be effective in determining $\eta(T)$ from Eq. (1). We have performed standard MD simulations using a periodic cubic simulation cell containing 500–2048 atoms. After equilibration is attained, typically in 100 000 time steps, the simulation is allowed to proceed for a buffer period of 10 000 iterations without any temperature control. The stress autocorrelation function is then averaged over 2000 sets in the *NVE* ensemble and 8–12 independent runs.

Figure 7 shows the MD results with the viscosity and the temperature expressed in reduced units appropriate to the BLJ potential (see Sec. II). In implementing Eq. (6) we take each local minimum given by the TSP trajectory in Fig. 4 to be the energy of a node, and the transition frequency a_{ij} in Eq. (3) is then specified by the activation barrier q_{ij} as labeled in Fig. 4. In implementing Eq. (9) we take the effective activation barrier $\bar{Q}(T)$ determined in Appendix B (see Fig. 15). To set the Network model and SPA results in the form for comparison with MD we choose to normalize the viscosities at $T=1$. Figure 7 shows the Network model matches well with the MD data. We regard this as the most important result of our benchmarking, a confirmation that our formulation of the Green–Kubo formalism to incorporate activated state kinetics indeed captures the temperature variation of the

viscosity determined by MD (in the region where the latter is expected to be valid). Additionally the SPA formulation describes a viscosity increase with lower temperature that is too strong compared to the MD and the Network model. This can be understood as a direct consequence of our activation barrier analysis (Appendix B) where $\bar{Q}(T)$ is obtained as an upper-bound estimate. We can therefore attribute the difference between the Network model and SPA results as the effects of activation path coupling which are treated in the former but not in the latter. These observations, seen in the low-viscosity region, should also hold in the high-viscosity region where we next test our formulations against experimental data on fragile liquids.

VI. VISCOSITY OF VISCOUS LIQUIDS: CALCULATIONS AND EXPERIMENTS

In comparing the Network model and SPA results with experimental data we adopt a different normalization from the preceding comparison with MD. Recall that the normalization amounts to assigning a numerical value to the frequency ν_o in Eq. (3), or the prefactor η_o in Eq. (9). Given that the experimental data for a number of fragile liquids all extrapolate at high temperature to a viscosity of 10^{-5} Pa s (see Fig. 8 below) it seems appropriate to use this value as the high temperature limit in normalizing the Network model and SPA results. In Fig. 8 the two theoretical results for $\eta(T)$ are now shown in absolute units along with a collection of experimental measurements on fragile liquids,[25] with temperature scaled in T_g, the glass transition temperature defined operationally as $\eta(T_g)=10^{12}$ Pa s. For the experimental data the T_g of each liquid is of course known, while for the two theoretical curves we use the T_g value of 0.37 in reduced unit given by Eq. (6).[20] Since there are no viscosity calculations giving results anywhere near 10^{12} Pa s for the BLJ model (or any interatomic potential for that matter), there is no way to directly validate our value of T_g. On the other hand, the mode-coupling theory temperature T_c for the BLJ model has been estimated to be $T_c=0.435$.[8] This gives a value for the ratio $T_c/T_g \sim 1.3$, consistent with what is considered to be a general rule of thumb.[25]

In comparing the Network model and SPA with experimental data on fragile liquids we are primarily interested in understanding the characteristic non-Arrhenius behavior of these liquids. Since the SPA formulation is simpler and more physically transparent, we consider its results first, as shown in Fig. 8(a). We see Eq. (9), with a temperature-dependent effective activation barrier determined in Appendix B, describes the "fragile" behavior exhibited by the data points in a qualitatively similar manner. It provides a smooth transition from a modest increase with decreasing temperature in the low-viscosity range to a strong increase through the high-viscosity range. On the other hand, in a more quantitative sense the SPA results clearly lie on the high side of the band of measured viscosities. We believe the lack of quantitative agreement is not surprising because the activation barrier $\bar{Q}(T)$ is expected *a priori* to be an upper-bound estimate along with ignoring coupling effects. Based on this reasoning we would expect the Network model formulation to provide

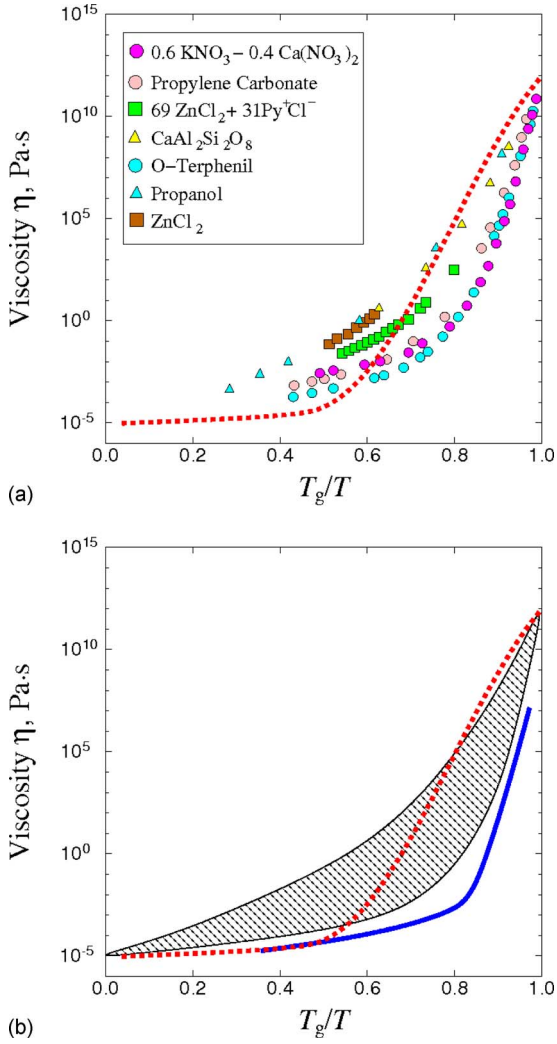

FIG. 8. (Color online) Experimental test of calculated viscosity for a BLJ potential model using the Network model [Eq. (6)] and SPA formulation [Eq. (9)]. (a) Comparison of SPA (dashed curve) with experimental data (Ref. 25) indicated by various symbols. (b) Comparison of Network model (solid curve) with experimental data (now shown as a band), along with SPA (dashed curve). For the calculated results T_g is 0.37 in reduced unit.

a correction in the direction of the experimental data. The implementation of Eq. (6) using the TSP trajectory discussed in Sec. III is not straightforward in that we have found the evaluation of the $\mathbf{A}(\omega)$ matrix is sensitive to the sampling robustness of the trajectory; a full discussion of this analysis will be reported in a companion publication.[20] Here Fig. 8(b) shows the calculated values of $\eta(T)$ down to a temperature where $\eta \sim 10^{10}$ Pa s. The agreement between the Network model and experiments is considered quite satisfactory given the ambiguity in the correspondence between any of the fragile liquids and the BLJ interatomic potential model. The model is seen to indeed describe a more pronounced fragile behavior similar to that indicated by the band of experimental data. From the standpoint of molecular studies of transport phenomena, our results demonstrate a way to go beyond the capabilities of MD simulation. In a follow-up study on molten silica, known to be a strong liquid, additional comparisons between simulation results and experiments will provide a further test of our two formulations.[26]

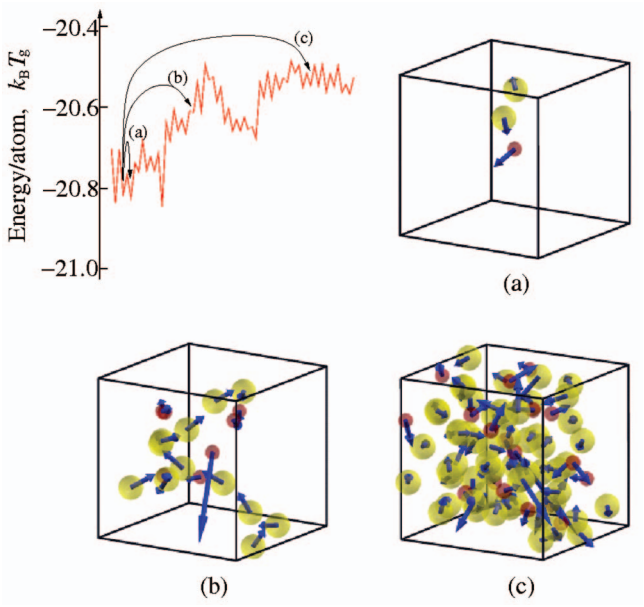

FIG. 9. (Color) Largest atomic displacements (indicated by arrows) associated with selected activation events as indicated on the TSP trajectory, (a) low-energy activation, (b) intermediate-energy activation, (c) high energy activation. Larger circles denote particle *A*, the majority species, and smaller circles denote particle *B*.

VII. DISCUSSION

An advantage of an atomistic method is that one can use appropriate interatomic interaction potentials to study different physical systems. Another significant advantage is the availability of atomic configurations which potentially can give insight into mechanisms of activation and relaxation. For the TSP trajectory shown in Fig. 4 we could look at the atomic displacements at any point along the trajectory. We discuss briefly such a result to show that details of the system behavior at the microscopic level can be obtained to correlate with macroscopic-level behavior in terms of the viscosity. The changes in atomic displacements (arrows) associated with three selected barrier climbing events are shown in Fig. 9. One sees that low-Q activation involves only a few atoms, while at higher Q, chainlike collective displacements can be seen, and at even higher Q rearrangements return to a more chaotic fashion. While these limited snapshots are by no means definitive, they appear to be consistent with recent investigations of the mechanisms of hopping between metabasins.[27,28]

Information of this kind, when combined with topographical features of the TSP trajectory discussed in Fig. 6, could lead to broader understanding of the kinetics of slow system evolution. More work in this direction would be worthwhile.

In summary, we propose a TSP trajectory sampling algorithm to be used in conjunction with two complementary methods of calculating the viscosity of highly viscous liquids. Of paramount concern throughout this work is the validity of our basin-filling algorithm, the activation barrier analysis, and the formulations to calculate viscosity in the high-viscosity range. We have addressed these concerns at three stages in presenting our results. We have benchmarked the algorithm by applying it to the problem of adatom diffusion on a metal surface, discussed in Sec. III with details given in Appendix A. Regarding the two formulations for computing the viscosity, the Network model and SPA, we first compared to MD simulations in the low-viscosity region, as shown in Fig. 7. Then we compared to experimental data in the high-viscosity region, as shown in Fig. 8. In both cases the Network model is found to be quite accurate, while SPA is able to account for the characteristic fragile scaling behavior in a qualitative manner. Additionally the coarse-grained temperature-dependent activation barrier $\bar{Q}(T)$ has been tested against experimental results in Fig. 16.

Because this work is the first of a four-part study aimed at calculating liquid viscosity in the range $(1-10^{12}$ Pa s), there are further results to report. Part 2 is a parallel study applying the approach described here to a potential model for silica, a system with measured viscosity that follows closely an Arrhenius behavior.[26] It turns out that the combination of the two studies allows further interpretations of the nature of fragility behavior in supercooled liquids. Part 3 is a full exposition of the Network model study and examination of its relation to the SPA formulation, including corrections for entropic effects.[20] Part 4 is devoted to detailed comparison of the present activated kinetics approach to calculating viscosity with the traditional MD approach and showing in the process that a crossover from strong to fragile behavior can occur in the low-viscosity range.[29] Taken together, our findings suggest that fragility, with its fundamental connection to current understanding of the dynamics of glass transition,[11,30,31] is a universal manifestation of all systems undergoing slow deformational changes. We believe there is no qualitative distinction between strong versus fragile liquids—even the so-called strong liquids should show a fragile-to-strong transition, although at high temperature and over a smaller range. Such a point of view has been raised from the perspective of spatial scales in glassy systems.[31]

ACKNOWLEDGMENTS

We thank L. J. Button, S-H Chen, S. Raghavan, D. C. Allan, and A. Rovelstad for thoughtful discussions. We also thank G. Henkelman and T. Rye for useful advice in running the Al surface diffusion simulations. This work was supported by Corning Incorporated, with additional support from Honda R&D Co., Ltd., NSF TeraGrid under Grant No. DMR-080064, DMR-090073, and DMR-090079, and Boston University Scientific Computing and Visualization. J.L. acknowledges support by the NSF under Grant No. CMMI-0728069, AFOSR under Grant No. F49620-1-0447, ONR under Grant No. N00014-05-1-0504, and Ohio Supercomputer Center.

APPENDIX A: BENCHMARKING BASIN FILLING ALGORITHM

A suitable test problem to validate our sampling method is atomic diffusion on a metal surface[32] for which results are available from previous simulation studies.[33–35] We choose a standard model[36] consisting of six Al (001) layers, each with 50 atoms, and one Al adatom. With two bottom layers kept

TABLE I. Calculated activation barrier Q and number of Gaussian penalty functions used to escape from initial energy minimum for different combinations of Gaussian width σ^2 and height W.

σ^2 (Å^2)	W (eV)	Q (eV)	n_g
1.0	0.01	0.43	148
0.8	0.2	0.55	8
0.6	0.1	0.25	12
0.6	0.01	0.235	104
0.6	0.005	0.229	215

fixed, the simulation cell has $3N=603$ degrees of freedom. Interatomic interactions are described by an Embedded Atom Method (EAM) potential.[37] Table I shows the calculated activation barriers and the corresponding number of penalty functions needed to locate the saddle point for several combinations of (σ^2, W) values. One sees that larger activation volume allows the adatom to escape from the initial minimum in fewer steps and generally overestimates the barrier, whereas lower activation energy gives more accurate barriers but requiring more steps. Even though the atomic configurations at each saddle point differ slightly, in all cases activation occurs through the knock-out mechanism found by Feibelman[32] and depicted in Fig. 10(a). The activation barrier sampled by using 215 Gaussian penalty functions with $\sigma^2=0.6$ Å^2 and $W=0.005$ eV is 0.229 eV. This may be compared to 0.227 eV given by the dimer method[7] by conducting 10^3 searches and comparing the activation energy of each saddle point obtained. In contrast, the present result is obtained in a single run.

The effectiveness in saddle point determination is further illustrated by considering the diffusion of a cluster of adatoms where the activation mechanism could not be easily anticipated by intuition. We again choose a standard model consisting of six Pt(111) layers, with 56 atoms per layer, and a 7-adatom cluster.[36] Three bottom layers are fixed so the number of degrees of freedom is $3N=525$. Interatomic interactions are in the form of Morse potential with parameters chosen to reproduce the diffusion barrier on Pt surfaces.[38] This case offers an opportunity to illustrate another feature of the algorithm, the flexibility to activate any subspace of the full $3N+1-D$ space. For example, if we decide to activate a single corner atom in the adcluster, $3N=3$, we would find an activation energy of 1.695 eV, as shown in Fig. 10(b). On the other hand, applying penalty functions to the top three layers and the cluster, with $3N=525$, we obtained a much lower activation barrier of 0.604 eV, with cluster migration process shown in Fig. 10(c). In the second case the process involved 63 penalty functions with $\sigma^2=1.0$ Å^2 and $W=0.05$ eV. For both cases the activation barriers agree with the results given by the dimer method, 1.693 eV (Ref. 36) and 0.601 eV,[34] respectively.

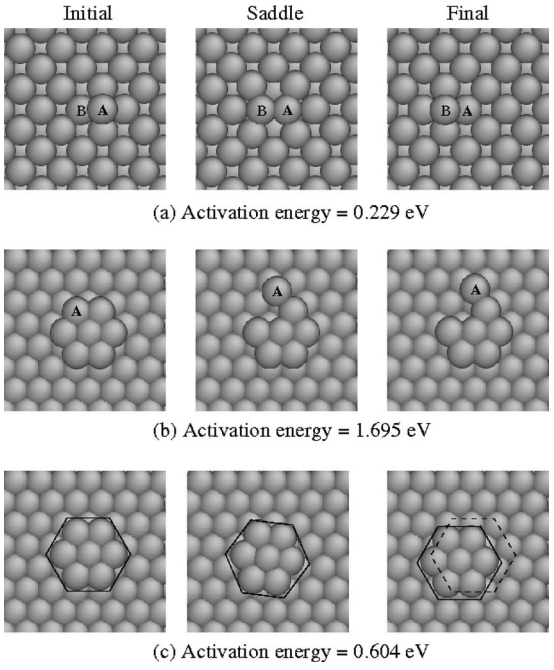

FIG. 10. (a) Activation of Al adatom on (100) surface. Adatom A knocks out atom B in the first layer and taking its position. (b) Activation of Pt adatom island on (111) surface when only atom A is penalized. (c) All seven atoms in the island and top three surface layers are penalized.

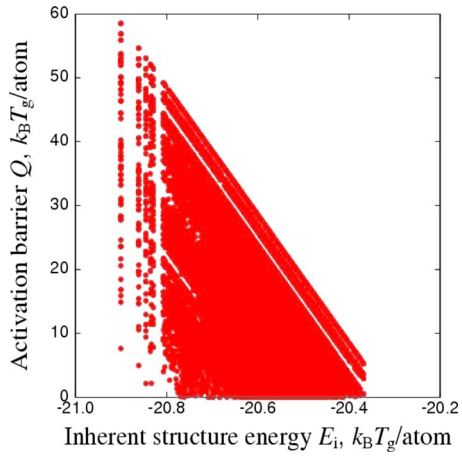

FIG. 11. (Color online) Scatter plot of values of q_{jk} extracted from the trajectory shown in Fig. 4. A point is shown for each E_j^m that has a value E_i and all the E_k^m that can be connected by an activation energy q_{jk}. Because points on top of each other do not show up, the number of k states that can be connected is not displayed in this plot.

APPENDIX B: ACTIVATION BARRIER DETERMINATION

We have developed a statistical analysis of the connectivity among the local minima by focusing on the activation energy q_{jk} indicated in Fig. 4. Our purpose is to extract an effective (coarse-grained) activation barrier in the sense of transition state theory, a quantity that describes how structural relaxation in the system varies with temperature. As illustrated in Fig. 4 the activation energy q_{jk} is the amount of energy required to connect an arbitrary pair of local minima j and k. Its value $Q \equiv q_{jk}$ is not unique because there can be different pairs of minima connected by the same value of activation energy. The degeneracy holds also for the energy of a local minimum; there can be a number of $E_{\min}^{(j)}$ all having the same value, say E_i. By considering all possible ways of connecting a pair of local minima, we can generate from Fig. 4 the following scatter plot. On the x-axis we label the en-

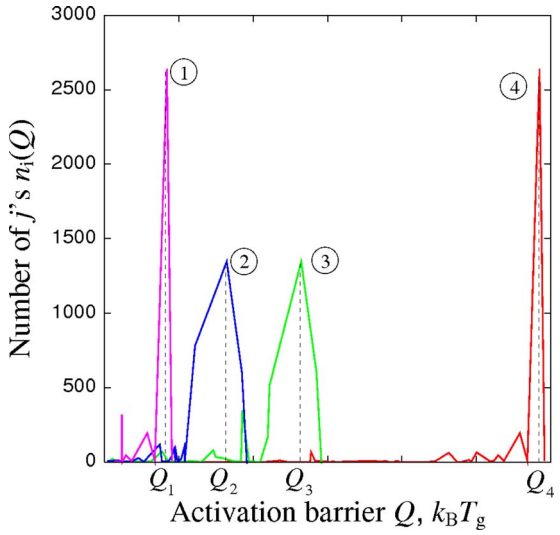

FIG. 12. (Color online) Distributions of number of local minima k that the system can reach with activation energy Q starting in local minima j with energy E_i. Four distributions are shown corresponding to energies E_i shown in Fig. 13. The E_i values for the distributions 1, 2, 3, and 4 are −20.4, −20.5, −20.6, and $-20.9k_BT_g$, respectively. T_g is 0.37 in reduced unit.

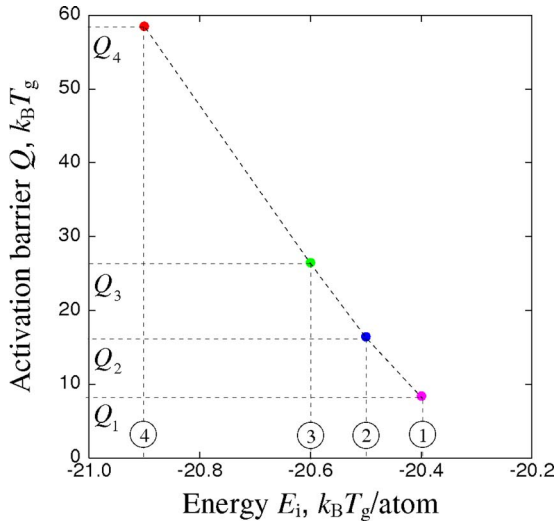

FIG. 13. (Color online) Q-E_i cross plot for four discrete values of E_i. See text for explanation. T_g is 0.37 in reduced unit.

ergy of the initial local minimum j for a given j. On the y-axis we plot the value of q_{jk} for a given k. This gives one point on the plot. Now imagine we repeat this process for all the j's and k's in Fig. 4. The result is then the scatter plot, Fig. 11. There are points in the plot that occur more than once, but one cannot see this. What one can see is the outline of the points. Along the x-axis the highest value of $E_{\min}^{(j)}$ corresponds to the smallest value of a local minimum (most shallow well). At this E_i value the activation energies q_{jk} are spread over a narrow range of low values. At the opposite end of the E_i values (deepest well), the range of q_{jk} is much greater. Figure 11 does not show which points are degenerate and what is the degeneracy. This information, the density of points (number of j's and k's), is more readily seen from a density of states or density distribution plot, Fig. 12.

Let $n(Q|E_i)$ be the number of local minima k that can be connected to E_i with activation energy Q. If we let Q be a variable, then $n(Q|E_i)$ can be regarded as a distribution in Q for various values of E_i. For the sake of illustration we consider four discrete values of E_i. Figure 12 shows the four distributions, with high and low values of E_i (shallow and deep potential well) indicated by 1 and 4, respectively, and the intermediate values denoted by 2 and 3.

Notice that the distributions are sharply peaked at the two ends of the E_i range. For high E_i the peak (high density of states) occurs at low Q values, while for low E_i the peak is at high Q values. If we take the Q values at the maximum of the distributions, and cross plot these Q's against the corresponding values of E_i, we would obtain the four points shown in Fig. 13. Thus the statistical analysis of our trajectory data shows two kinds of connectivity. Following the high density of states one can trace out a curve showing that one can hop between shallow wells at low activation, and between deep wells at high activation, see Fig. 13.

Connecting the four points in Fig. 13 gives a relation between an activation barrier and the depth of the potential well. Because the Q values in Fig. 13 correspond to the maximum in $n(Q|E_i)$, the relation also implies a large number of intermediate steps are involved in the activation process. In other words, using this relation to describe the variation of activation energy with well depth is appropriate for a highly cooperative process, one involving many degrees of freedom in the system (collective rather than individual). One can consider other parts of the cross plot. For example, at low Q and low E_i, one finds configurations much different from the high Q and low E_i point in Fig. 13 (see Fig. 14 below). Carrying out the same analysis described in Figs. 12 and 13 for all the E_i values from different sampling trajectories, we obtain the three-dimensional plot shown in Fig. 14. We have chosen the initial configurations of the samplings from the inherent structures database generated in Sec. II. The inherent structures with different energies are selected to cover the range of quench probability calculation in Fig. 2(b).

Figure 14 depicts the variation of the activation barrier Q with the value of the initial local minimum (well depth,

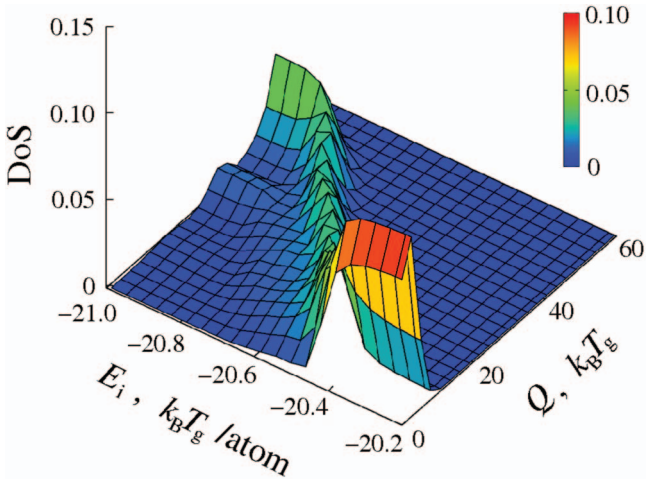

FIG. 14. (Color) Density distribution of Q for different E_i (color coded). T_g is 0.37 in reduced unit.

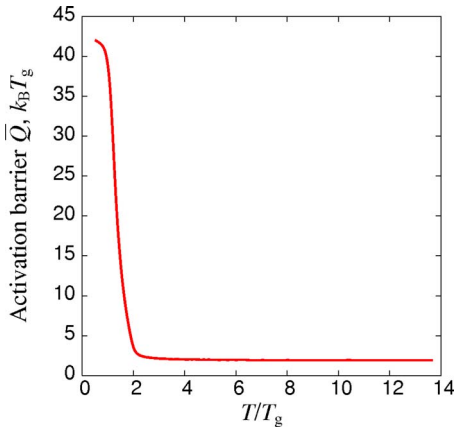

FIG. 15. (Color online) Temperature variation of the coarse-grained activation barrier $\bar{Q}(T)$ obtained by combining the high density path shown in Fig. 14 with the average inherent structure shown in Fig. 2(b). T_g is 0.37 in reduced unit.

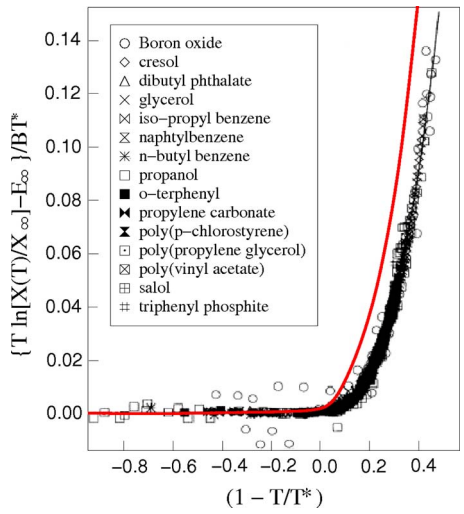

FIG. 16. (Color online) Experimental test of the coarse-grained temperature-dependent activation barrier of Fig. 15 (solid curve) against scaled activation barriers derived from viscosity measurements (various symbols) (Ref. 39). Except for scaling the axes no adjustable parameters are involved in the comparison.

higher energy means shallower well). For shallow wells Q is low in value and insensitive to well depth variation. As the well becomes deeper, Q increases in value and is sensitive to well depth variation. Taking the "ridge" path in Fig. 14 as a characteristic relation between Q and E_i, we introduce a coarse graining and mapping procedure to deduce a temperature-dependent effective activation barrier $\bar{Q}(T)$. Coarse graining here means we replace Q by an effective barrier $\bar{Q}$ with the same dependence on E_i, and replace E_i by the average inherent structure energy $\bar{E}(\alpha)$. Mapping means we write $\bar{Q}(\bar{E})=\bar{Q}(T)$, and the barrier is now associated with the temperature at which initial inherent structure configuration for the basin-filling sampling is generated. The result of this procedure is shown in Fig. 15.

We see that $\bar{Q}(T)$ is constant at high T but rises sharply as T decreases below a characteristic value. What we have observed in Fig. 14 is even more accentuated. The increase in activation has two contributions. From Fig. 14 we have seen that the activation energy rises when the local minimum decreases to a certain value. The nature of this increase is activated state kinetics. From Fig. 2 we see that $\bar{\alpha}$ decreases sharply with T below $T\sim 0.6$. The nature of this decrease is thermodynamic (inherent structure scaling with temperature).

Being a coarse-grain quantity, $\bar{Q}(T)$ can be compared to temperature dependence of activation barriers extracted from experiments. Such results have been obtained by fitting viscosity data on a number of fragile glass-forming liquids to a formula with three constants.[39] We have used the same formula to fit our $\bar{Q}(T)$ result given in Fig. 15, thereby determining the values of the three constants (T^*, B, and E_∞ in Ref. 39). This particular way of representing our calculations is shown (solid curve) in Fig. 16. Also shown for comparison are the actual experimental data (symbols, line drawn through the data is to guide the eye). At high temperatures the barrier is constant at a low value, implying little activation is needed to explore the PES landscape. Beyond the plateau region, $\bar{Q}(T)$ rises sharply. Since the binary LJ model is not meant to describe quantitatively any of the liquids in the data, only a qualitative comparison of the overall behavior of the activation barrier is meaningful. Figure 16 may be regarded as a first experimental test of our approach to computing viscosity of supercooled liquids, starting with the basin-filling method and ending with the determination of the effective activation barrier for structural relaxation, Secs. II–IV. It is clear that there is an agreement between the predicted result and those derived from experiments. Moreover, the difference brought out by the comparison can be understood as a consequence of our upper-bound estimate of $\bar{Q}(T)$. In other words the predicted behavior is expected to show generally stronger activation than the experiments.

[1] C. A. Angell, Science **267**, 1924 (1995).
[2] T. S. Grigera, A. Cavagna, I. Giardina, and G. Parisi, Phys. Rev. Lett. **88**, 055502 (2002).
[3] D. Coslovich and G. Pasotore, J. Chem. Phys. **127**, 124505 (2007).
[4] F. H. Stillinger and T. A. Weber, Phys. Rev. A **25**, 978 (1982).
[5] A. Laio and M. Parrinello, Proc. Natl. Acad. Sci. U.S.A. **99**, 12562 (2002).
[6] R. Martonak, A. Laio, and M. Parrinello, Phys. Rev. Lett. **90**, 075503 (2003).
[7] G. Henkelman and H. Jonsson, J. Chem. Phys. **111**, 7010 (1999).
[8] W. Kob and H. C. Andersen, Phys. Rev. E **51**, 4626 (1995).
[9] F. H. Stillinger, Science **267**, 1935 (1995).
[10] S. Sastry, P. G. Debenedetti, and F. H. Stillinger, Nature (London) **393**, 554 (1998).
[11] G. Debenedetti and F. H. Stillinger, Nature (London) **410**, 259 (2001).
[12] F. H. Stillinger and T. A. Weber, Phys. Rev. A **25**, 978 (1982).
[13] O. M. Becker and M. Karplus, J. Chem. Phys. **106**, 1495 (1997).
[14] J. C. Mauro, R. J. Loucks, J. Balakrishnan, and S. Raghavan, J. Chem. Phys. **126**, 194103 (2007).
[15] F. Wang and D. P. Landau, Phys. Rev. Lett. **86**, 2050 (2001).
[16] H. Löwen, Phys. Rep. **237**, 249 (1994).
[17] C. P. Massen and J. P. K. Doye, Phys. Rev. E **75**, 037101 (2007).
[18] D. A. McQuarrie, *Statistical Mechanics* (Harper & Row, New York, 1973), p. 512.
[19] G. A. Fernandez, J. Vrabec, and H. Hasse, Fluid Phase Equilib. **221**, 157 (2004).
[20] J. Li, J. Chem. Phys. (to be published).
[21] S. G. Brush, Chem. Rev. (Washington, D.C.) **62**, 513 (1962).
[22] E. N da C. Andrade, Nature (London) **125**, 309 (1930).
[23] G. Adam and J. H. Gibbs, J. Chem. Phys. **43**, 139 (1965).

[24] A. Heuer, J. Phys.: Condens. Matter **20**, 373101 (2008).
[25] C. A. Angell, J. Phys. Chem. Solids **49**, 863 (1988).
[26] A. Kushima, X. Lin, J. Li, J. Eapen, X. Qian, J. C. Mauro, P. Diep, S. Yip, J. Chem. Phys. (to be published).
[27] G. A. Appignanesi, J. A. Rodriguez Fris, R. A. Motani, and W. Kob, Phys. Rev. Lett. **96**, 057801 (2006).
[28] B. Doliwa and A. Heuer, Phys. Rev. E **67**, 031506 (2003).
[29] J. Eapen, A. Kushima, J. Li, and S. Yip, J. Chem. Phys. (to be published).
[30] J. C. Dyre, Rev. Mod. Phys. **78**, 953 (2006).
[31] K. Trachenko and V. V. Brazhkin, J. Phys.: Condens. Matter **20**, 075103 (2008).
[32] P. J. Feibelman, Phys. Rev. Lett. **65**, 729 (1990).
[33] A. F. Voter, Phys. Rev. Lett. **78**, 3908 (1997).
[34] G. Henkelman, G. Johannesson, and H. Jonsson, in *Progress on Theoretical Chemistry and Physics*, edited by S. D. Schwartz (Kluwar, Dordrecht, 2000), p. 269.
[35] D. Passerone and M. Parrinello, Phys. Rev. Lett. **87**, 108302 (2001).
[36] R. A. Olsen, G. J. Kroes, G. Henkelman, A. Arnaldsson, and H. Jonsson, J. Chem. Phys. **121**, 9776 (2004).
[37] A. F. Voter and S. P. Chen, Mater. Res. Soc. Symp. Proc. **82**, 2384 (1987).
[38] D. W. Bassett and P. R. Webber, Surf. Sci. **70**, 520 (1978).
[39] D. Kivelson, G. Tarjus, X. Zhao, and S. A. Kivelson, Phys. Rev. E **53**, 751 (1996).